

## Nanocavity in a silicon waveguide for ultrasensitive nanoparticle detection

Bradley Schmidt,<sup>a)</sup> Wilson Almeida, Christina Manolatu, Stefan Preble, and Michal Lipson  
*School of Electrical and Computer Engineering, Cornell University, Ithaca, New York 14853*

(Received 17 February 2004; accepted 16 September 2004)

We demonstrate the use of a micron-size planar silicon photonic device for the detection of ultralow concentrations of metal nanoparticles. The high detection sensitivity is achieved by using a strong light confining structure that enhances the effective extinction cross section of metal nanoparticles. We demonstrate the detection of 10 nm diameter gold particles with a density of fewer than 1.25 particles per  $0.04 \mu\text{m}^2$ . Using such a device one could detect the presence of single metal nanoparticles specifically bound to various analytes, enabling ultrasensitive detection of analytes including DNA, RNA, proteins, and antigens. © 2004 American Institute of Physics.  
 [DOI: 10.1063/1.1819997]

There is a growing need for the development of environmental, health safety, and clinical microfabricated biosensors for many analytes such as DNA, RNA, proteins, antigens, and other biomolecules, which allow for lower cost, smaller sample volumes, massive parallelism, and ultrahigh sensitivity.<sup>1-3</sup> Many of these biosensing systems rely on binding the analyte to individual label particles, such as quantum dots, gold particles, and fluorescent dye molecules. Current systems for ultrasensitive biodetection<sup>4-6</sup> using these labels are either complex, large, or lack the desired level of sensitivity. The challenge of improving the sensitivity of integrated systems is due to the low cross section (emission or absorption) of the labels that are often bound to the analyte.

In this letter we report results demonstrating a high degree of detection sensitivity of nanoparticles using a submicron size silicon integrated structure on a chip. This sensitivity is achieved by using a strong light confining nanocavity structure that enhances the effective extinction cross section of metal nanoparticles. As a result of the strong light confinement, precisely where the particle is located, the presence of a single metal nanoparticle with a diameter as small as 10 nm can be detected by measuring the decrease in transmission of light propagating through the photonic structure. Gold particles are used here as a sensing probe due to their large extinction coefficient in the wavelength range of interest (1450–1600 nm) and their mature use as labels in biosensing systems.<sup>7</sup>

The structure is a one-dimensional photonic crystal<sup>8</sup> consisting of a high index contrast silicon waveguide (450 nm wide, 250 nm in height) with 200 nm diameter holes filled with a lower index material (silicon dioxide with  $n=1.46$ ) in the waveguide to create distributed Bragg reflectors (DBRs) on either side of a 910 nm long cavity. A small 100 nm diameter  $\text{SiO}_2$  nanocavity (filled hole) is embedded in the center of the microcavity. The addition of this defect at the center of the cavity creates a local discontinuity in the field, increasing the strength of the field in the center of the cavity.<sup>9</sup> Sample devices were fabricated using silicon on insulator (SOI) wafers with 250 nm of crystalline silicon on top of a  $3 \mu\text{m}$  thick buried oxide layer. The structure was defined using electron-beam lithography using FOx-12 spin-on glass as a negative resist and etch mask and etched

by chlorine based reactive ion etching (RIE). The holes were filled and the structure clad with  $\text{SiO}_2$  using plasma enhanced chemical vapor deposition.

Figure 1 shows the 3D finite difference time domain (FDTD) simulations of the structure. Due to the light confinement in the cavity and the presence of the small nanocavity, a strong field (TE-like mode) is present in the center of the device, which is  $\sim 315$  times stronger than the field inside the core of the regular waveguide. The field enhancement induces a strong enhancement of the effective extinction cross section of the metal nanoparticle. A side cross section of the 3D FDTD simulations [Fig. 1(b)] shows that the field at the top surface of the central nanocavity is relatively strong, approximately half the magnitude of the field at the center depth of the nanocavity. This indicates that the top surface of the cavity can be used as a sensor without the need to embed the nanoparticles inside the waveguide in order to be detected. The small out of plane radiation also enables us to perform relatively accurate 2D simulations on the structure as opposed to 3D. The device was chosen to have a quality factor  $Q=190$ . This  $Q$  enhances the cross section of the chosen size of metal nanoparticle in order to allow the clear detection of single particles, without being too sensitive to fluctuations in environmental conditions, and to the exact position of the particle.

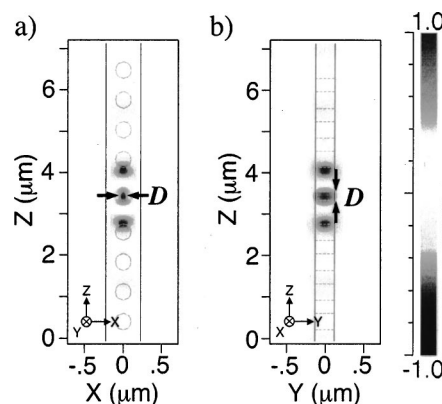


FIG. 1. TE-like mode field profile of the field inside the microcavity with 100 nm diameter nanocavity  $D(n=1.46)$  at resonance wavelength  $\lambda = 1.568 \mu\text{m}$ ; (a) top view center cross section, (b) side view center cross section.

<sup>a)</sup>Electronic mail: bss15@cornell.edu

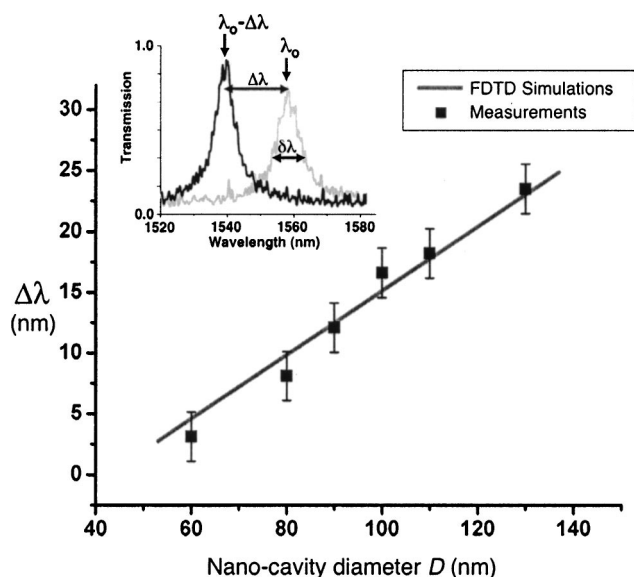


FIG. 2. Experimental results and FDTD simulations for the relative shift in resonance due to the presence of the nanocavity as a function of nanocavity diameter. Inset shows transmission spectra of two devices with different nanocavity diameters.

In order to verify that the field in the device is indeed localized in the center of the cavity and to investigate the degree of confinement, we measured the spectral response of several fabricated devices, all having the same dimensions except for varying the diameter  $D$  of the central nanocavity. Figure 2 shows the relative shift of the spectral resonances of the microcavities due to the change in the diameter of the nanocavity. The inset of Fig. 2 shows transmission spectra of two devices, each with a different nanocavity diameter. The quality factor  $Q$  of the devices ( $\lambda_0/\delta\lambda$ ), equal to the ratio of the energy stored in the device at resonance to the energy lost per cycle of oscillation is equal to  $\sim 182.3$ . The strong dependence of the spectra due to the very small variation in the size of the nanocavity indicates that the field is strongly confined within this small region. The experimental results closely match our 2D simulation results, showing that the resonance shift due to the varying nanocavity diameters correspond to those predicted by FDTD calculations (solid line) of  $\Delta\lambda/D=0.263$ .

We measured the transmission losses due to the presence of gold metal nanoparticles, using the same devices with a 100 nm diameter nanocavity. Due to the requirement of having a top cladding for the optimal operation of our fiber to waveguide couplers<sup>10</sup> the upper cladding was only removed above the cavity devices. The upper cladding was removed by patterning 20  $\mu\text{m}$  diameter holes using photolithography. It was etched close to the surface of the cavity using  $\text{CHF}_3$  based RIE, followed by highly selective HF wet chemistry in order to remove the remaining cladding down to the top surface above the cavity without allowing possible roughness from the RIE process. Once the cavities were exposed, the transmission through the devices was measured with water and various depositions of colloidal gold particles on top of the cavities. These depositions were achieved by placing small amounts of water-based solutions of 10 nm gold particles ( $1.9 \times 10^{13}$  particles per ml) on top of the devices and allowing them to dry by evaporation. Each deposition step deposited  $\sim 30.0$  particles per micron<sup>2</sup> on the entire structure, corresponding to  $\sim 1.25 \pm 0.2$  particles in the sensing area of

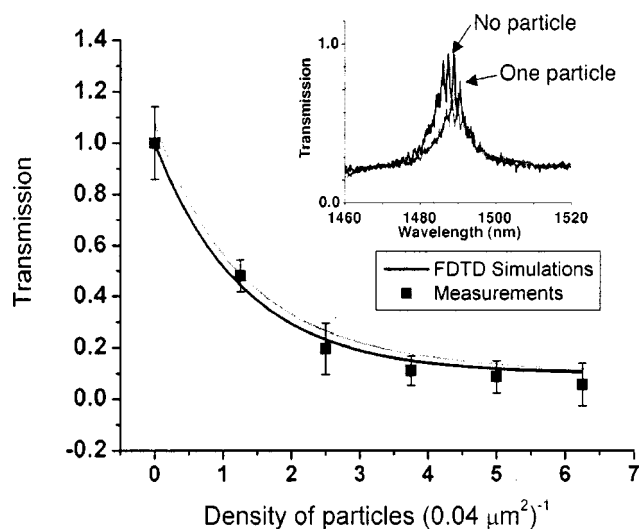


FIG. 3. Normalized transmission as a function of the number of particles within the sensing area of  $0.04 \mu\text{m}^2$ . Inset shows the transmission measured for no particles on the structure, and for one particle in the sensing area.

$0.04 \mu\text{m}^2$  per additional deposition step. After each evaporation, the device was again covered in water. Careful placement allow the particles to remain settled on the surface while transmission measurements were made. The optical sensing area is calculated as the area of the top surface of the device weighted by the field intensities in each region. Figure 3 shows the measured transmission as a function of the number of nanoparticles deposited in the optical sensing area. The error bars represent deviation from the average measured value due to the processing and temperature variation in our experiments. The inset of Fig. 3 shows the spectra measured for no particles on the structure and for one particle in the optical sensing area. A strong decrease in transmission was observed with increasing number of particles, with a drop in transmission of as much as 52% for the addition of the first deposition of particles on the sensing area.

In order to theoretically analyze the structure as a sensor we consider the presence of gold nanoparticles in our 2D FDTD simulations by assuming that they are bound to the top surface of the cavity, as is the case in our experiment. These simulations assumed that the top oxide cladding had been replaced with water to replicate our experimental setup. The top of the structure is assumed to be unclad and covered by water ( $n=1.33$  and  $k=1.48 \times 10^{-4}$ , at  $25^\circ\text{C}$  and at a wavelength of 1550 nm). Figure 3 shows that a large decrease in expected transmission intensity per additional particle is observed (solid black line) in agreement with our experimental results. The error bars in the theoretical curve represent the deviation from the average value due to variations in the particle position. FDTD simulations also predict low losses due to scattering from the particle on the top surface of the waveguide. A difference in forward scattering and lateral scattering between the device with and without the particle is less than 0.02%, and 0.6%, respectively, confirming that the transmission decrease is mainly due to the absorption by the particle.

Due to the characteristic modal volume of this cavity along with the presence of the low index nanocavity in the center of the microcavity, the gradient of the field is small over the area of the selected sensing region. Therefore similar results were achieved when the particles in the simulation

were randomly placed away from the center, but still on the top surface of the nanocavity, resulting in less than a 2% change in absorption losses as compared to when the particles were placed only in the very center of the sensing area. This change is shown as the gray solid line in Fig. 3.

In conclusion, we have demonstrated a planar integrated micron-size photonic device that enables sensing of a discrete number of metal nanoparticles. Using such a device, one could detect the presence of a single metal nanoparticle specifically bound to various analytes, enabling massively parallel ultrasensitive detection of analytes including DNA, RNA, proteins, and antigens on chip.

The authors would like to acknowledge the support of the Cornell Center for Materials Research (CCMR) with funding from the Materials Research Science and Engineering Center Program of the National Science Foundation (Contract No. DMR-0079992) and the STC Program of the National Science Foundation (Contract No. DMR-0120967). This work was performed in part at the Cornell Nano-Scale

Science and Technology Facility (a member of the National Nanofabrication Users Network) which is supported by the National Science Foundation under Grant No. ECS-9731293, its users, Cornell University, and Industrial Affiliates.

- <sup>1</sup>L. R. Huang, J. O. Tegenfeldt, J. J. Kraeft, J. C. Sturm, R. H. Austin, E. C. Cox, *Nat. Biotechnol.* **20**, 1048 (2002).
- <sup>2</sup>J. R. Epstein, A. P. K. Leung, K.-H. Lee, and D. R. Walt, *Biosens. Bioelectron.* **18**, 541 (2003).
- <sup>3</sup>G. Wu, R. H. Datar, K. M. Hansen, T. Thundat, R. J. Cote, and A. Majumdar, *Nat. Biotechnol.* **19**, 856 (2001).
- <sup>4</sup>A. J. Haes and R. P. Van Duyne, *J. Am. Chem. Soc.* **124**, 10596 (2002).
- <sup>5</sup>S. Nie and R. Emory, *Science* **275**, 1102 (1997).
- <sup>6</sup>V. S.-Y. Lin, K. Moteshari, K.-P. S. Dancil, M. J. Sailor, and M. R. Ghadiri, *Science* **278**, 840 (1997).
- <sup>7</sup>I. Alexandre, S. Hamels, S. Dufour, J. Collet, N. Zammateo, F. De Longueville, J. L. Gala, and J. Remacle, *Anal. Biochem.* **295**, 1 (2001).
- <sup>8</sup>J. S. Foresi, P. R. Villeneuve, J. Ferrera, E. R. Thoen, G. Steinmeyer, S. Fan, J. D. Joannopoulos, L. C. Kimerling, H. I. Smith, and E. P. Ippen, *Nature (London)* **390**, 143 (1997).
- <sup>9</sup>V. R. Almeida, Q. Xu, C. A. Barrios, and M. Lipson, *Opt. Lett.* **29**, 1209 (2004).
- <sup>10</sup>V. R. Almeida, R. Panepucci, and M. Lipson, *Opt. Lett.* **28**, 1302 (2003).